ORIGINAL ARTICLE

Luminol-Modified Graphene Quantum Dots as an Efficient Nano-Sensor for Fe $^{3+}$ Sensing in Aqueous Solution

Noura H. Harran[1] · Bassam F. Alfarhani[1]

Abstract

Graphene quantum dots (GQDs) are a distinct type of fluorescent material with zero dimensions and are highly valued for their exceptional quantum confinement, optical size, and characteristics. A simple alkaline hydrothermal process achieved a surface modification of Graphene Quantum dots (GQDs) with Luminol to enhance the fluorescence emission and hence the better limit of detection. Their structural information was obtained using Fourier transform infrared spectroscopy (FTIR), transmission electron microscopy (TEM), photoluminescence spectroscopy, X-ray diffraction (XRD), and UV-Vis absorption spectroscopy. The results demonstrated that the GQDs had a consistent size distribution ranging from 6 to 18 nm and possessed an abundance of nitrogen-containing functional groups. The modified graphene quantum dot (GQD) has significant optical characteristics, including a tenfold increase in fluorescence intensity. The altered graphene quantum dots (GQDs) were employed to detect ferrous ions (Fe^{3+}) in an aqueous solution. It exhibits remarkable selectivity for (Fe^{3+}) compared to other metal ions in an aqueous solution. The fluorescence intensity exhibited an inverse relationship with the concentration of (Fe^{3+}) ions. The calibration curve displayed linear regression (R^2) within the given concentration range of 0.21–300 µMolar. The detection limit was determined to be 0.08 µM. The results demonstrate that Luminol-GQDs, functioning as a photoluminescence sensing platform, possess the necessary selectivity for environmental applications and can effectively detect (Fe^{3+}) ions in the presence of other ions in aqueous samples.
.

Keywords Graphene quantum dots · Fluorescence · Fe3 + detection and fluorescence quenching

1 Introduction

GQDs (graphene quantum dots) are a new member of the organic compound/graphene family and fluorescence-affected compounds and have achieved notable research interest. As a result of the distinct quantum edge and confinement effects, GQDs show unique electrical and optical phenomena among several types of quantum dots. [1–7] In contrast to semiconductor quantum dots, GQDs show noticeably high thermal conductivity, stable photoluminescence, excellent solubility, better surface grafting, low toxicity, high stability, and high electrical conductivity, thus turning them into compounds with high potential in fluorescent probe fields, cell imaging, optoelectronic devices, etc. [8–14]. Graphene quantum dots (GQDs) have been developed as a new fluorescent probe platform sensing different analytes [15–18]. Several sensors have been used based on the fluorescence quenching mechanism of GQDs [19–22]. Fe^{3+} ions detection by selective fluorescence quenching of GQDs was first reported on by Wang et al. [23]. Fe^{3+} is a crucial metal ion existing in biological and environmental systems. Fe^{3+} ions can interact with several materials in biological systems, such as proteins. The concentration of Fe^{3+} ions plays a crucial role in the control of PD (Parkinson's disease), as the neurons of PD patients will be affected by the accumulation of Fe^{3+} ions [24].

Additionally, Fe^{3+} ions are among the significant chemicals in the environmental system that act as pollutants and pollute water [25]. Due to the above reasons, selective and sensitive Fe^{3+} ions detection is urgently required. Electrochemical sensing and Instrumental detection usually involve complicated sample preparations with limited reliability and

✉ Bassam F. Alfarhani
bassam.alfarhani@qu.edu.iq

[1] Department of Chemistry, College of Science, University of Al-Qadisiyah, Diwaniah city, Iraq

reproducibility [26, 27]. Hence, the sensitive and straightforward detection by GQDs as a fluorescence-based approach makes GQDs a very effective tool for quantitative and qualitative monitoring of harmful ions in the environmental system. However, the GQDs show a considerably low value of LOD (limit of detection) for detecting Fe^{3+} ions owing to the limited number of surface active sites [28].

The active sites on the GQDs have been enhanced to reduce this effect. For example, amino groups (e.g., amine N) functionalized GQDs will deliver active sites with high abundance, which produce superiority in detecting Fe^{3+} ions. Moreover, the smaller size of GQDs and narrower size distribution were achieved by the effect of passivation of the surface via a particular surfactant, showing an increase in a specific surface area [29]. The detection performance for Fe^{3+} ions was enhanced, resulting from the increasing specific surface area of the GQDs due to the large number of active sites; thus, the effect functionalization of GQDs with amine N groups and surface passivation can cause an active sites improvement, which may play a significant role in the Fe^{3+} enhancement and detection limit. [30]

In this work, we develop a luminol functionalized GQD fluorescent material probe for exhibiting an excellent response for Fe^{3+} detection. The modified GQD is easily synthesized through one-step hydrothermal synthesis using citric acid as a precursor. The as-prepared L-pGQDs (Luminol- Trimethoxy(propyl)silane-GQD) have uniform size and a single-layered graphene structure. In addition, L-pGQDs have bright light blue fluorescence. The presence of Fe^{3+} ions sensitively quenched the fluorescence intensity of the Luminol-pGQD (L-pGQD), whereas other metal ions, such as Ni^{2+}, Ag^{+}, Cd^{2+}, Na^{+}, K^{+}, $Mg^{2+,}$ and Pb^{2+} could hardly quench it. This assay might provide a new pathway for detecting Fe^{3+} ions and some potential applications in biological systems and environments.

2 Methodology

2.1 Chemicals

Citric acid monohydrate (99.5-100.5%), sodium hydroxide (98%), Trimethoxy(propyl)silane (97%), luminol (97%), potassium chloride (99-100.5%), and Fe^{3+} chloride hexahydrate (97%) were all purchased from Sigma-Aldrich, Sodium chloride from scharlau, lead nitrate, hydrochloric acid 35–38%, nickel chloride hexahydrate, silver nitrate, Aluminium Sulphate, Chromium(III) chloride hexahydrate, magnesium chloride, Cadmium nitrate from BDHwith analytical purity and utilized as received without further purification. Ultra-pure water was used in all experiments with 18MΩ resistivity.

2.2 Instrumentation

Ultraviolet-visible (Uv-vis) absorption spectra were measured using a UV-1800 spectrophotometer (Shimadzu). All steady-state fluorescence measurements were carried out with a fluorescence spectroscopy RF-5301PC (Shimadzu, Japan) at room temperature. The aqueous solutions of GQDs were placed in a cuvette made with quartz, and all windows were polished using 5 nm slit-width for excitation and emission monochromators. The Fourier transform infrared(FTIR) spectra were obtained on an FT-IR spectrophotometer (TENSOR 27, Bruker). X-ray powder diffraction (XRD) patterns were performed by Aeris-Benchtop X-ray Diffractometers (Malvern Panalytical).

Raman spectra were recorded in Raman thermo nicolet Raman spectrometer USA, with a laser excitation wavelength of 785 nm. The size and morphology of GQDs were performed using transmission electron microscopy (TEM) using a 100KV electron microscope Philips model: CM120. SEM data were obtained using (Axia ChemiSEM, Netherlands).

2.3 Synthesis of GQDs

The GQDs were prepared by direct citric acid pyrolyzing. First, 2.10 g of mono-citric acid was heated to 200 °C using a hotplate. Five minutes later, the citric acid was liquated, and a colour change was observed to be pale yellow and turn into a reddish-orange colour collide GQDs. Notice that further heating times must be avoided instead of generating dark graphene oxide. The reddish-orange liquid was added dropwise into 4 mg mL-1 NaOH solution under vigorous stirring for 10 min until thoroughly mixed. After mixing, the solution was neutralized by adding HCl drops (10 mg mL-1) to obtain pH 7, a yellowish-green compound. The GQDs solution was filtered using a syringe filter (0.22 μm pore size) to remove the residual reagents, and the obtained filtrate was then collected and dialyzed using a 1000Da dialysis bag for 8 h. Freeze-dring was done for the obtained solution to obtain GQDs powder.

2.4 Synthesis of L-pGQDs

0.2 mL of trimethoxy(propyl)silane (TMPS) was added to 100 mL of the GQDs solution, and the mixture was stirred for 24 h at room temperature and was then freeze-dried to obtain pGQDs powder. Then, Luminol- pGQDs, pGQDs (2 mg ml-1), and luminol were added to sodium hydroxide (4 mg ml-1) followed by 30 min ultrasonic treatment. Then, the resulting mixture is transferred into a polytetrafluoroethylene-lined autoclave, followed by a reaction at 180 °C for 8 h. After cooling to room temperature, the product was

filtered using a syringe filter with a 0.22 μm pore size and followed by freeze-drying to obtain L-pGQD power.

2.5 Detection Procedure for Fe(III) ions

Stock standard solutions 2.7 mg ml^{-1} Fe^{3+} were prepared by dissolving an appropriate amount of FeCl$_3$.6H$_2$O, and the volume of water was adjusted to 500 mL in a volumetric flask followed by further dilution to known concentrations using stepwise preparation.

Following a systematic approach, a known concentration of L-pGQDs was transferred to a four-polished side fluorescent cuvette. The fluorescent intensity of the solution was meticulously recorded from 200 to 600 nm, with an excitation wavelength fixed at a wavelength that shows the highest intensity in the nanometer. After an appropriate amount of Fe^{3+} ions were added, the intensity of fluorescence of the solution was recorded. This procedure was then repeated for various pre-determined concentrations of Fe^{3+} ions and other metal ions, ensuring the reliability of the results. For comparison, the L-pGQDs solution volume was fixed to be 2 mL before adding Fe^{3+}, and the working solutions and measurements were all at room temperature.

3 Results and Discussion

3.1 Morphological Analysis and Characterization

The morphology and structure of L-pGQD were investigated by s field emission scanning electron microscopy (FESEM) and transmission electron microscope (TEM). The low electro-contrast between the carbon-coated TEM grids and GQDs makes the high-quality TEM images challenging to obtain, and some nanosheets of 9 nm in size can still be noticed. The GQDs with a size of about 9 nm and spherical morphology with the size distribution can be seen

in the image in Fig. 1. The size of GQDs was distributed in a narrow range of 6~18 nm.

Field-emission scanning electron microscopy (FESEM) is an advanced imaging technique that can be used to study the surface morphology and topography of graphene quantum dots (GQDs) at high resolution; FESEM image of GQDs typically shows a cluster of small, spherical-shaped particles with a size range of a few nanometers. The surface morphology and texture of the particles can vary depending on the method of synthesis and processing. EDX-mapping estimated the element's compositions and dispersion. A high-resolution surface morphology shown by the FESEM technique underlines the variance in the GQDs and pGQDs surface texture, suggesting element distribution. The chemical composition of citric acid and the obtained GQDs was determined by energy dispersive X-ray (EDX) spectroscopy [34]. Figure 2. Shows the results with a high percentage of carbon of 29.7% (Fig. 2.c) compared to oxygen percentages of 42% (Fig. 2.b) in GQDs representing the carbonization of citric acid and the formation of GQDs. GQDs pose a uniform circular shape. The NaOH solution employed in the synthesis shows a Na peak in GQDs. The SEM image (Fig. 2.a) shows average particle size around 13. 77 nm.

Figure 3 shows the XRD patterns of GQDs with three prominent diffraction peaks. The peak at $2\theta = 27.8$ deg corresponds to the (002) plane of the graphite, and the peaks at $2\theta = 32.2$ and 45.8 deg corresponds to the (100) & (102) planes. [31, 32] The three diffraction peaks are relatively sharp, which proves that the prepared GQDs have good crystallinity. Scherrer's equation was employed to estimate the nanoparticles' average size, L, in the prepared samples. According to Scherrer's equation $D = K\lambda/\beta\cos\theta$, where the constant $K = 0.943$, the x-ray wavelength $\lambda = 0.15405$ nm, the diffraction peak half-height width $\beta = 0.257$, and the diffraction angle $\theta = 13.4$ deg, the calculated grain size D is equal to 33.4 nm. However, for the sample with a small particle size, the grain size deduced by XRD is larger than

Fig. 1 Show TEM analysis (**a**) TEM image of the Quantum dot and, (**b**) size distribution of the synthesized particles
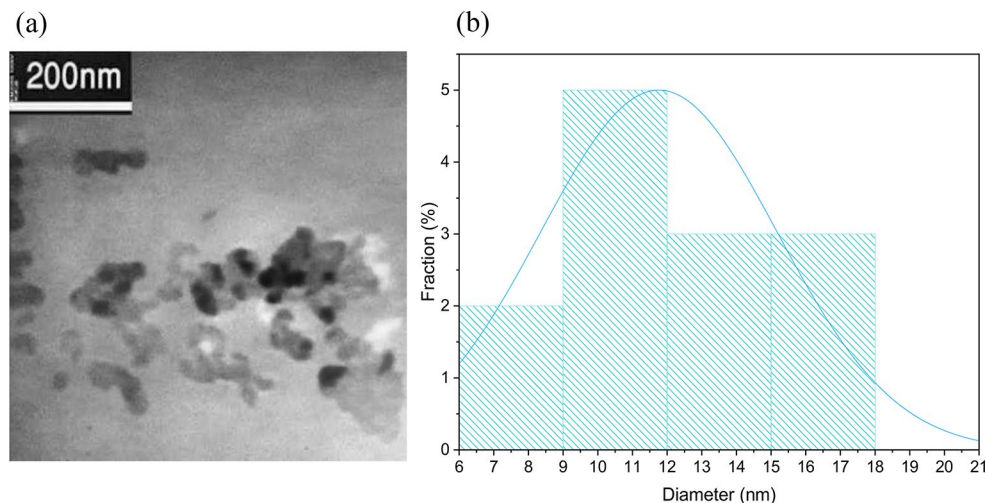
Fig. 2 shows; (**a**) SEM image of GQD (**b**) and (**c**) the EDX image of carbon and oxygen percentages respectively, and (**d**) the distribution of the elements in the sample
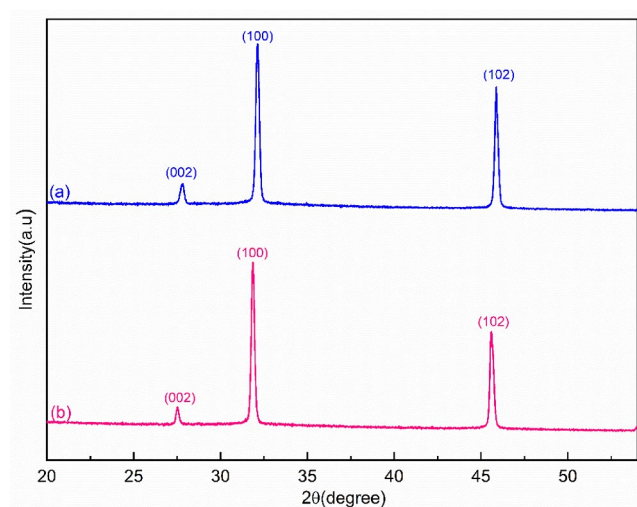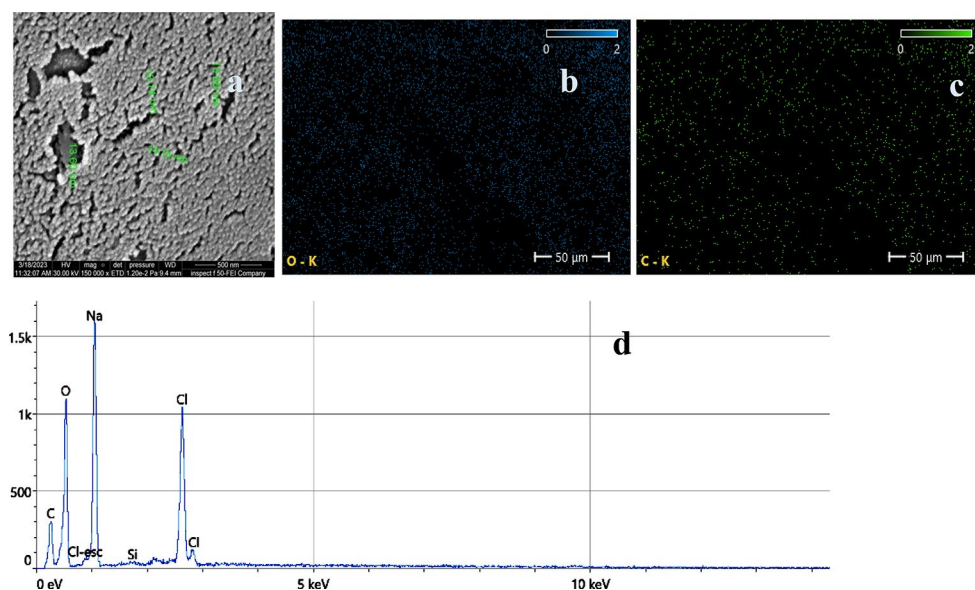

Fig. 3 XRD pattern for (**a**) GQDs and (**c**) pGQDs

Fig. 4 FTIR spectra of (**a**) pGQDs, (**b**) Luminol and (**c**) Luminol-pGQDs

the actual size. When the particle size is < 10 nm, the surface has multiple grain boundaries. XRD cannot distinguish between these two boundaries, so the actual size of some samples can be smaller than the value calculated by the Scherrer formula.

The crystallinity and structure of the modified GQDs were measured using XRD. The XRD pattern of GQDs showed peaks close to 2θ value of 27.8°, 32.21° and 45.87°, which matched to (002), (100), and (102) planes of hexagonal carbon [28]. The minor change in peaks of the GQDs crystal structure was observed upon modification with trimethoxy(propyl)silane, which suggested modification of the GQDs with pGQDs, showing the pattern of GQDs.

A broad peak near 2θ value of 23.16° was observed in the XRD pattern of GQDs, which is related to the d-spacing of 3.84 Å of (002) plane of graphite or layer-to-layer distance.
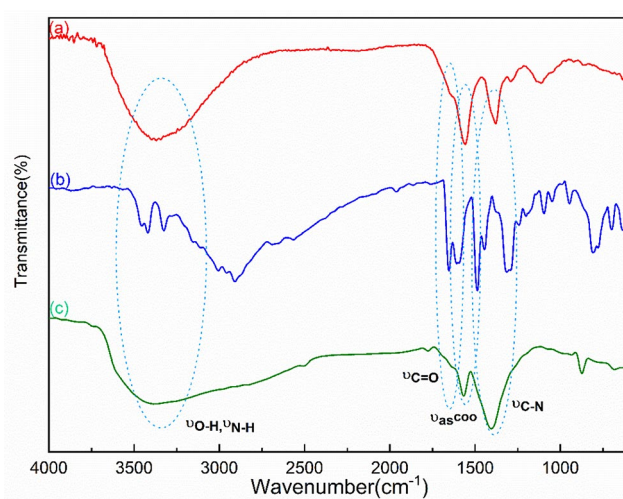
This finding is significant as it provides insights into the layered structure of GQDs. Additionally, there are two other peaks at 31.8° and 45.8° which correspond to (100) and (102) planes of hexagonal carbon, respectively.

The ATR-FTIR spectra of pGQD are given in Fig. 4. Trimethoxy (propyl) silane was used to functionalize the GQDs with propyl groups and Exhibited broad peaks absorption carboxyl groups around 1376.20 cm^{-1} and 1550.49 cm^{-1} attributed to the symmetric and asymmetric carboxyl group stretching vibrations, respectively and Stretching vibration of C-OH in around 1351 cm^{-1} and broadband around 3347.19 cm^{-1} attributed to O-H stretching vibration of hydroxyl groups. For aromatic compounds, the results show no characteristic absorption bands (C–H stretching vibration in aromatic rings of around 3000–3100 cm^{-1} and skeletal vibration of aromatic rings in a range of 1450–1650 cm^{-1}
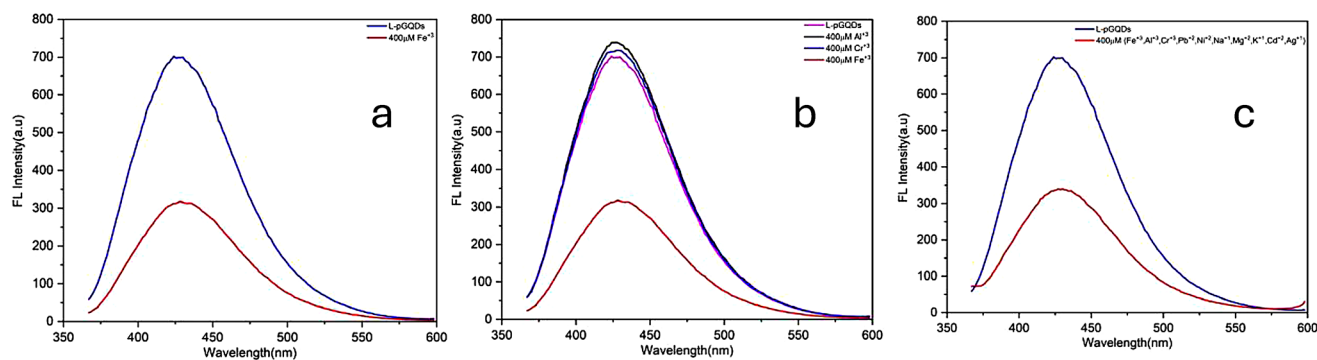
Fig. 5 represents the fluorescence intensity of modified GQD (**a**) presence of 400μM Fe^{3+}, (**b**) intensity of GQD and selected divalent ions with and without Fe^{3+} and (**c**) intensity of GQD and selected divalent and trivalent ions with and without Fe^{3+}

) the resulting spectra, show that the absence of aromatic compound is in the obtained GQDs. After surface modification with (trimethoxy)propyl silane (pGQDs), a broad peak around 1122 cm^{-1} can be assigned to the Si-O-C asymmetric stretching vibration speculating the successful silylation of GQDs. Modification with luminol shows the presence of C=O and asymmetric carboxyl group bonds around 1638, and 1564 cm^{-1}, respectively, moreover, abroad peak at about 3500 cm^{-1} corresponded to the stretching vibration of N-H bond in luminol and O-H bond in pGQDs.

1401 cm^{-1} obtained band was a C–N absorption and The appearance of a 3115 cm^{-1} was linked to the N–H stretching vibration of amine groups, indicating the successful incorporation of nitrogen atoms (from luminol) into the pGQDs.

3.2 Selective Detection of Fe^{3+} ion

The selective sensing of Fe^{3+} was performed using ex/em equal to 304/428 nm with pH = 7.4 phosphate Buffer saline solution containing L-pGQDs (0.12 g in 50 ml) and 400 μM concentration of different ions such as Pb^{2+}, Ni^{2+}, Na^+, Mg^{2+}, K^+, Cd^{2+}, Al^{3+}, and Cr^{3+} with ionic radii equal to 1.29, 0.45, 1.12, 0.66, 1.46, 0.95, 0.55, 1.02, 0.51 and 0.61 nm respectively. The fluorescence spectra in Fig. 5a demonstrate a significant decrease in intensity when Fe^{3+} ions are present. This result is consistent when adding other trivalent ions, as shown in Fig. 5b These findings reveal the selective detection of Fe^{3+} ions among the chosen trivalent ions. Figure 5c displays the fluorescence intensity of the modified GQD when exposed to a combination of divalent and trivalent ions, both with and without the addition of Fe^{3+}.

Fe^{3+} ion was characterized by a smaller ionic radius which makes faster and more stable interaction with Luminol-GQD and smaller hydration energy (-4430 kJ mol^{-1}) compared with −1485, -2105, -406, 1922, -322, -1807, -413, -413 and −4060 kJ mol^{-1} for Pb^{2+}, Ni^{2+}, Na^+, Mg^{2+}, K^+, Cd^{2+} Al^{3+}, and Cr^{3+} respectively [33].
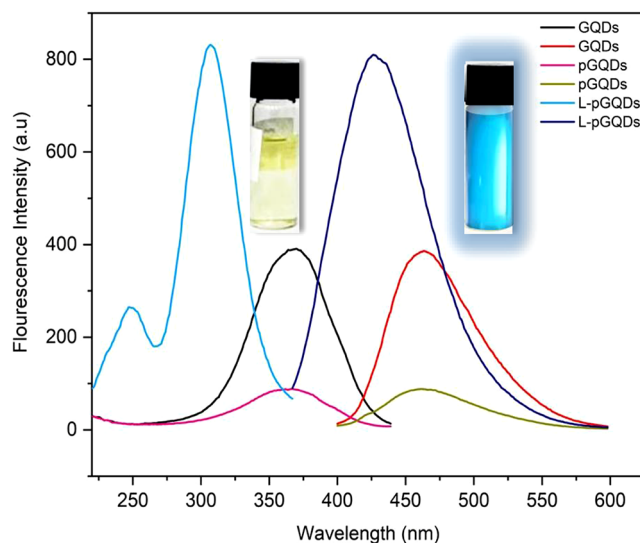

Fig. 6 Ex/Em spectra of GQD, pGQD and L-pGQD

The L-pGQD shows significant fluorescence at a specific wavelength of emission when excited by a 304 nm wavelength. As a result, the presence of metal ions was detected using this particular wavelength. Then, the fluorescence intensity levels of L-pGQD were analyzed after adding various metal ions. Figure 6, shows that the fluorescence signal of L-pGQDs was notably reduced only by the Fe^{3+} ion compared to other metal ions in the sample.

These findings indicate that Fe^{3+} can be detected with high selectivity using L-pGQD. The quenching of PL results from Fe^{3+} ions that strongly attract the amino group of L-pGQD and form a stable complex. To explain the detection system's mechanism, a Stern–Volmer relationship was used to demonstrate the dependence of luminescence intensity of L-pGQDs on Fe^{3+} ions with different concentrations. The Stern–Volmer analysis depicted in Fig. 7 illustrates the relationship between $(F0/F)-1$ and $[Fe^{3+}]$, where F0 represents the PL intensity of the blank sample, and F represents the PL intensity with various metal ion concentrations. It is
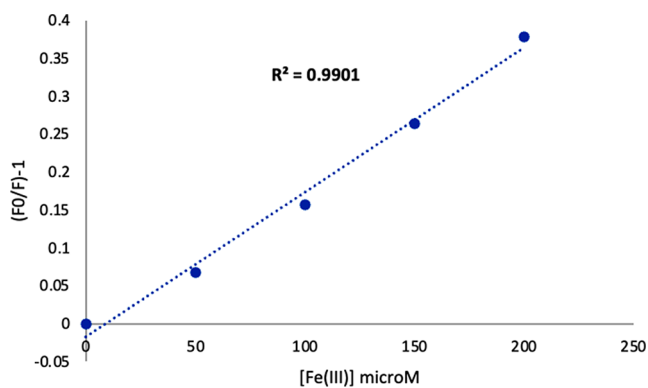
Fig. 7 Plot of Stern–Volmer equation relating F0(intensity with no quencher and F the Fluorescence intensity with the quencher)

worth noting that a linear relationship was observed in the Stern–Volmer Plot within the Fe^{3+} ion concentration range of 50–300 μM. This suggests that the charge transfer mechanism between GQDs and Fe^{3+} ions may involve a static mechanism.

The affinity of various metal ions toward L-pGQD was conducted under consistent experimental conditions. The results in Fig. 8 indicate that Fe^{3+} ions display the highest affinity for L-pGQD compared to other metal ions, indicating the potential for selective sensing by L-PGQD. Additional research was conducted to examine how the concentration of Fe^{3+} affects the fluorescence intensity of GQDs. The PL spectra of L-pGQD with varying concentrations of Fe^{3+} can be seen in Fig. 9. These spectra demonstrate that the amount of Fe^{3+} present highly influences the PL intensity of L-pGQD. As the concentration of Fe^{3+} increases, the PL intensity decreases.

A rapid reduction in photoluminescence (PL) was noted when Fe^{3+} was introduced; the fluorescence quenching was tested at concentrations ranging from 1 to 300 μM of Fe^{3+}.
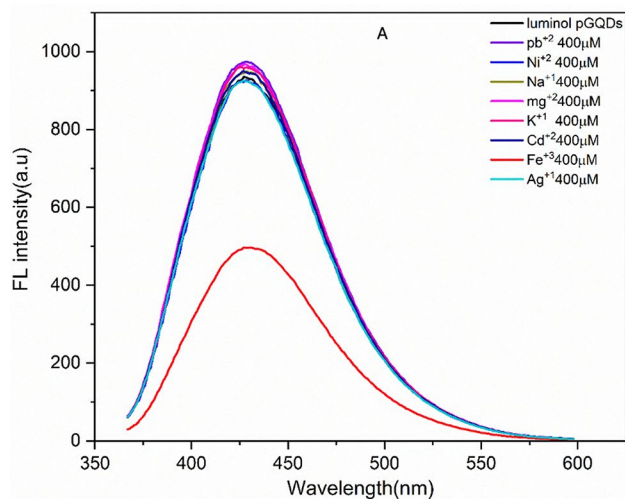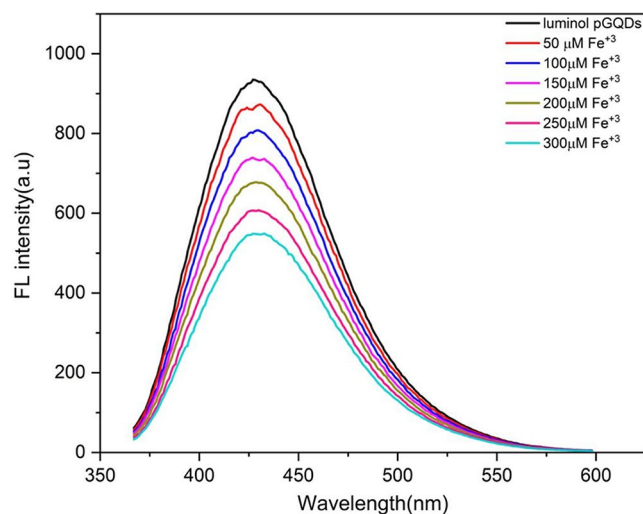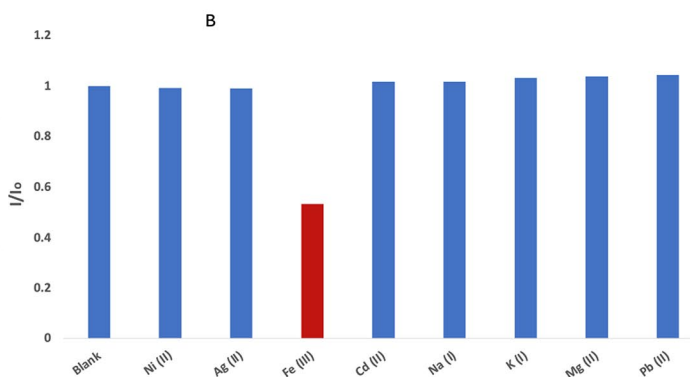

Fig. 9 Fluorescence spectra of L-PGQD with different concentrations of Fe^{3+}

An acceptable linear relationship was observed, as depicted in Fig. 10, with an excellent linear regression value (R^2) of 0.9901, indicating accurate detection of Fe^{3+} ion concentration. These findings suggest that the prepared L-pGQD can be a selective and sensitive sensor for detecting Fe^{3+} ions. The limit of detection (LOD, Eq. 1) and limit of quantification (LOQ, Eq. 2) were determined using the following formulas:

$$LOD = 3.3^* \sigma / S \qquad (1)$$

$$LOQ = 10 * \sigma / S \qquad (2)$$

Where σ represents the standard deviation of the 16 blank measurements, and the intercept represents the slope of the linear regression plot. It is denoted by S. The limits of

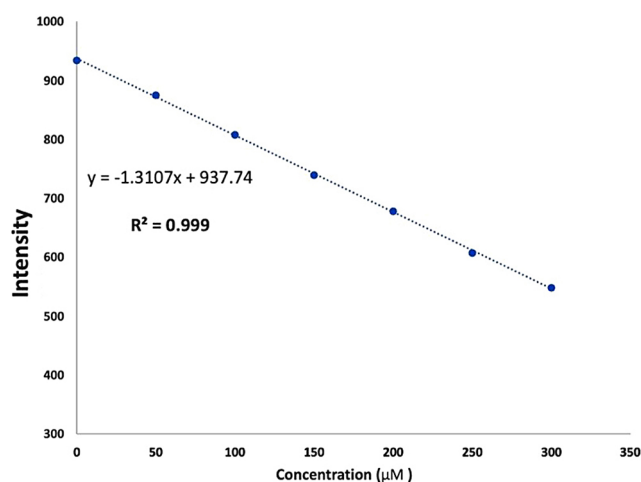

Fig. 8 (**a**) Fluorescence intensity quenching of L-PGQD in the presence of Fe^{3+}, (**b**) relative fluorescent intensities of the L-PGQD presence of different ions (blue column) and presence of Fe^{3+}ion (red column)

Fig. 10 linear relation between the fluorescence quenching efficiency and the concentrations of Fe^{3+} in the range of 50–300 μM

Table 1 Fe^{3+} ion detection by different carbon-based materials

Sensing probe	LOD (μM)	Ref
GQDs photoluminescence	7.22	[2]
CQDs(folic acid)	35	[16]
N-CQDs(chitosan, acetic acid and 1,2-ethylenediamine)	0.18	[17]
GO nanosheet	7.9	[18]
N-GQDs	0.09	[19]
B-CQDs(glucose and boric acid)	0.242	[20]
CQDs(citric acid and Tris)	1.3	[21]
N-GQDs(glycine and ethylene glycol)	0.1	[22]
Luminol-pGQDs nanocomposite	0.08	This work

detection (LOD) and quantification (LOQ) were determined to be 0.08 μM and 0.26 μM, respectively. The detection limit for Fe^{3+} in this research was significantly below the recommended concentration (5.36 μM) by the World Health Organization for drinking water, indicating the potential of L-PGQD in detecting small amounts of Fe^{3+}. Table 1 compares Fe^{3+} ion detection using different carbon-based materials as reported by researchers. The limit of detection achieved in this study is much lower than previously reported values for Fe^{3+} detection, signifying the great potential of L-PGQD in practical applications for sensing Fe^{3+}.

3.3 Method Greenness Assessment

The method of greenness was evaluated by NEMI (National Environmental Methods Index) [32]. GAC (Green analytical chemistry) is the term that drags the attention of any analytical chemist to keep in mind environmental safety and Health matters during any given experimental work. The term greenness of any analytical experiments and procedures is a group of parameters classified as complicated and
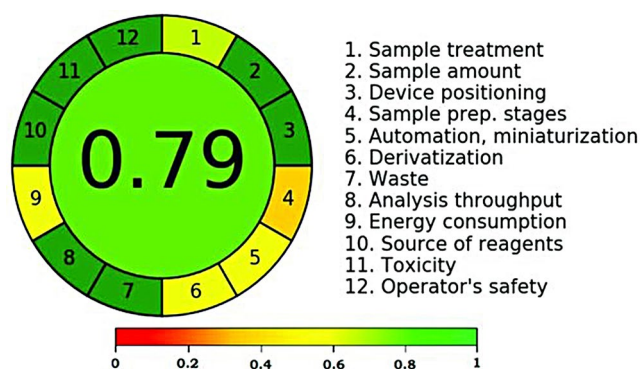

Fig. 11 NEMI (National Environmental Methods Index) [32].

not easily determined quantitatively. Numerous methods for Green analytical chemistry metrics have been established. The first described approach is NEMI, which is a metric system constructed on an easy-to-read pictogram, separated into 4 sections, representing reagents that are persistent, generation of waste bioaccumulative or toxic, whether the conditions are corrosive, and whether reagents are hazardous). The greenness of the suggested method is represented in Fig. 11 and shows an acceptable score of 65, which is considered a good score and conder as acceptable. Colour code: yellow, red, and green signifying medium, high and low influence on the environment, respectively.

4 Conclusion

A straightforward yet highly efficient fluorescent probe has been developed, L-pGQDs, specifically designed to detect Fe^{3+} ions. The probe exhibits a high degree of selectivity and minimal interference from other metal ions (Ni^{2+}, Ag^+, Cd^{2+}, Na^+, K^+, Mg^{2+}, Pb^{2+}, $Al^{3+,}$ and Cr^{3+}) when excited at a wavelength of 304 nm in an aqueous solution. The mean size of the obtained modified graphene quantum dots (GQD) ranged from 6 to 18 nm, exhibiting a highly uniform size dispersion. The relationship between the fluorescence intensity of L-pGQDs and the amounts of Fe^{3+} ions demonstrates a significant linear relationship within the 50 to 300 μM range, with a minimum detection limit of 0.08 μM. GQDs provide remarkable luminescence, affordability, solubility, and exceptional sensitivity in detecting even trace amounts of metal ions and biomolecules, making them an excellent choice for various sensing applications. The material has the potential to fulfill the specific criteria for environmental applications. It possesses sufficient sensitivity to detect Fe^{3+} ions in water samples from the environment, which is stated by the detection limit by the U.S. Environmental Protection Agency as 5.36 μM. Based on the fluorescence measurements, it can be concluded that the sensing mechanism of the L-pGQDs is due to the formation of a complex between

Fe^{3+} ions and L-pGQDs. The recombination process of L-pGQDs, both in the presence and absence of Fe^{3+} ions, provides further evidence that the quenching mechanism is mainly static.

Declarations

Ethical approval This article does not contain any studies with human participants or animals performed by any of the Authors.

Informed consent Not applicable.

Conflict of Interest Not applicable.

References

1. Novoselov KS, Geim AK, Morozov SV, Jiang D, Zhang Y, Dubonos SV et al (2004) Electric field effect in atomically thin carbon films. Science 306:666–669
2. Geim AK (2009) Graphene: status and prospects. Science 324:1530–1534
3. Li L, Wu G, Yang G, Peng J, Zhao J, Zhu JJ (2013) Focusing on luminescent graphenequantum dots: current status and future perspectives. Nanoscale 5:4015–4039
4. Alfarhani BF, Al-Mousawi RR, Aziz RS, Shingar FK (2021) Modified Nano Particles Method for Fluorescent Dye removal from aqueous samples. IOP Conf Series: Earth Environ Sci 790:1901–1913
5. Alfarhani BF, Hammza RA, Alzaidy AS (2021) Potential Effect of Solvent and Slit Width on Some Properties of Room Temperature Fluorescence of Hydroxy Polycyclic Aromatic Hydrocarbons. Chemical papers *75* (8) 4217–4223
6. Alfarhani B, Al-Tameemi M, Goicoechea HC, Barbosa F, Campiglia AD (2018) Direct Analysis of Benzo[a]pyrene metabolites with strong overlapping in both the spectral and lifetime domains. Microchem J 137:51–61
7. Alfarhani B, Al-tameemi M, Schenone AV, Goicoechea HC, Barbosa F, Campiglia AD (2016) Room temperature fluorescence spectroscopy of Benzo[a]Pyrene metabolites on Octadecyl extraction membranes. Microchem J 129:83–89
8. Shen J, Zhu Y, Chen C, Yang X, Li C (2011) Facile preparation and upconversion luminescence of graphene quantum dots. Chem Commun 47:2580–2582
9. Li L-L, Ji J, Fei R, Wang C-Z, Lu Q, Zhang J-R et al (2012) A facile microwave avenue to electrochemiluminescent two-color graphene quantum dots. Adv Funct Mater 22:2971–2979
10. Zhu S, Zhang J, Liu X, Li B, Wang X, Tang S et al (2012) Graphene quantum dots with controllable surface oxidation, tunable fluorescence and up-conversion emission. RSC Adv 2:2717
11. Zhu S, Zhang J, Qiao C, Tang S, Li Y, Yuan W et al (2011) Strongly green-photoluminescent graphene quantum dots for bioimaging applications. Chem Commun 47:6858–6860
12. Gupta V, Chaudhary N, Srivastava R, Sharma GD, Bhardwaj R, Chand S (2011) Luminscent graphene quantum dots for organic photovoltaic devices. J Am Chem Soc 133:9960–9963
13. Zhuo S, Shao M, Lee S-T (2012) Upconversion and downconversion fluorescent graphene quantum dots: ultrasonic preparation and photocatalysis. ACS Nano 6:1059–1064
14. Li Y, Hu Y, Zhao Y, Shi G, Deng L, Hou Y et al (2011) An electrochemical avenue to green-luminescent graphene quantum dots as potential electron-acceptors for photovoltaics. Adv Mater 23:776–780
15. Yang F, Zhao M, Zheng B, Xiao D, Wu L, Guo Y (2012) Influence of pH on the fluorescence properties of graphene quantum dots using ozonation pre-oxide hydrothermal synthesis. J Mater Chem 22:25471–25479
16. Pan D, Zhang J, Li Z, Wu M (2010) Hydrothermal route for cutting graphene sheets into blue-luminescent graphene quantum dots. Adv Mater 22:734–738
17. Ponomarenko LA, Schedin F, Katsnelson MI, Yang R, Hill EW, Novoselov KS et al (2008) Chaotic Dirac billiard in graphene quantum dots. Science 320:356–358
18. Son Y-W, Cohen ML, Louie SG (2006) Half-metallic graphene nanoribbons. Nature 444:347–349
19. Li X, Wang X, Zhang L, Lee S, Dai H (2008) Chemically derived, ultrasmooth graphene nanoribbon semiconductors. Science 319:1229–1232
20. Cui Y, Liu L, Shi M, Wang Y, Meng X, Chen Y, Huang Q, Liu C (2024) A review of advances in Graphene Quantum dots: from Preparation and Modification methods to application. J Carbon Res 10:7
21. Ritter KA, Lyding JW (2009) The influence of edge structure on the electronic properties of graphene quantum dots and nanoribbons. Nat Mater 8:235–242
22. Karami MH, Abdouss M, Rahdar A, Pandey S (2024) Graphene quantum dots: background, synthesis methods, and applications as nanocarrier in drug delivery and cancer treatment: an updated review. Inorg Chem Commun 161
23. Dharmadhikari B, Debnath D, Patra P (2023) Advances in Structural Modifications and Properties of Graphene Quantum Dots for Biomedical Applications American Chemical Society, 6 21358–21376
24. Huenchuguala S, Segura-Aguilar J (2023) On the role of Iron in Idiopathic Parkinson's Disease. Biomedicines 20:11–15
25. Chua SF, Nouri A, Mahmoudi E, Ang WL, Mohammad AW (2023) Modified-graphene quantum dot thin-film nanocomposite membrane for enhanced nanofiltration performance and antifouling properties: minimal incorporation. J Water Process Eng 15:201–233
26. Dutt S, Hamza I, Bartnikas TB (2022) Molecular mechanisms of Iron and Heme Metabolism. Annu Rev Nutr 42:311–335
27. Vogt A-CS, Arsiwala T, Mohsen M, Vogel M, Manolova V, Bachmann MF (2021) On Iron Metabolism and Its Regulation. *International Journal of Molecular Sciences.22 (* 4591
28. Koppenol W, Hider R (2019) Iron and redox cycling. Do's and don'ts. Free Radic Biol Med 133:3–10
29. Zhang M, Bai L, Shang W, Xie W, Ma H, Fu Y et al (2012) Facile synthesis of water-soluble, highly fluorescent graphene quantum dots as a robust biological label for stem cells. J Mater Chem 22:7461–7467
30. Manchala S, Tandava VSRK, Jampaiah D, Bhargava SK, Shanker V (2019) Novel and highly efficient strategy for the green synthesis of soluble graphene by aqueous polyphenol extracts of Eucalyptus bark and its applications in high-performance supercapacitors. ACS Sustain Chem Eng 7:11612–11620
31. Jiang K, Sun S, Zhang L, Wang Y, Cai C, Lin H (2015) Brightyellow-emissive N-doped carbon dots: preparation, cellular imaging, and bifunctional sensing. ACS Appl Mater Interfaces 7:23231–23238
32. NEMI-CBR www.nemi.gov/cbr
33. Azim SA, El-Kemary MA, El-Daly SA (1996) Fluorescence quenching and complexation behaviour of tetraphenylporphyrin with some divalent metal ions. J Chem Soc Faraday Trans 5:747–752

34. Pichitchai Pimpang R, Sumang, Choopun S (2018) Effect of concentration of citric acid on size and Optical properties of fluorescence Graphene Quantum dots prepared by tuning carbonization degree. Chiang Mai J Sci 45:2005–2014